Geophysical Research Letters

RESEARCH LETTER
10.1029/2022GL102271

Key Points:

- Unlike S, the densities of Ni, C, O and H mix ideally with liquid Fe at Mars' core conditions
- Of the light elements (LEs), C and S have the largest effects on the bulk sound velocity of liquid Fe
- To match the density of Mars' core, any Fe-X binary requires a substantial amount of LE (e.g., >30 wt% S)

Supporting Information:

Supporting Information may be found in the online version of this article.

Correspondence to:
D. Huang,
dongyang.huang@erdw.ethz.ch

Citation:
Huang, D., Li, Y., Khan, A., Sossi, P., Giardini, D., & Murakami, M. (2023). Thermoelastic properties of liquid Fe-rich alloys under martian core conditions. *Geophysical Research Letters*, *50*, e2022GL102271. https://doi.org/10.1029/2022GL102271

Received 23 NOV 2022
Accepted 8 MAR 2023

Thermoelastic Properties of Liquid Fe-Rich Alloys Under Martian Core Conditions

D. Huang[1], Y. Li[2], A. Khan[3], P. Sossi[1], D. Giardini[3], and M. Murakami[1]

[1]Institute of Geochemistry and Petrology, ETH Zürich, Zürich, Switzerland, [2]Deep Space Exploration Laboratory/CAS Key Laboratory of Crust-Mantle Materials and Environments, University of Science and Technology of China, Hefei, China, [3]Institute of Geophysics, ETH Zürich, Zürich, Switzerland

Abstract Seismic measurements made on Mars indicate that the liquid iron-nickel core is rich in light elements; however, the effects of these light components on the elasticity of Mars' core remain poorly constrained. Here, we calculate elastic properties of various liquid Fe-X (X = Ni, S, C, O and H) mixtures using ab initio molecular dynamics simulations. We find that, at martian core conditions, the addition of S and O most effectively decreases the density of liquid iron, followed by C and H, while Ni has a minimal effect. As for compressional sound velocity (Vp), C increases Vp of liquid Fe throughout Mars' core, while both S and O reduce Vp, the intensity of which diminishes with increasing pressure. Assuming a martian core made of a binary mixture, the seismically-inferred density would require the presence of at least 30 wt% S.

Plain Language Summary Planetary structure and chemical constitution is a product of the material from which it formed. As a planet assembles material and continues to grow, it undergoes melting, enabling heavy elements like Fe and Ni to settle toward the center of the planet to form a core. During core formation, liquid metals can incorporate light elements (LEs) such as S, C, O and H that lower the density of the core relative to pure Fe. The amounts of these LEs can be inferred from geophysical measurements such as seismology, an approach used to deduce the composition of Earth's core. Similar seismic measurements have been obtained for Mars with the InSight mission, which have allowed us to place limits on the mean density of Mars' core and its chemical make-up. Relative to Earth's core, Mars' core is significantly less dense, requiring the presence of considerable amounts of LEs. We performed simulations based on first principles to determine the elastic properties of various Fe-Ni-rich-LE mixtures that can be compared with those obtained from for example, InSight to place further constraints on its core composition, but can also be used for other planets such as Mercury and mid-sized exoplanets.

1. Introduction

Seismic measurements made as part of the InSight mission (Banerdt et al., 2020) indicate that Mars' core is large and light with radius and mean density ranging between 1,790 and 1,870 km and 5.7–6.3 g/cm^3, respectively (Drilleau et al., 2022; Durán et al., 2022; Khan et al., 2022; Stähler et al., 2021). Relative to pure liquid Fe (Kuwayama et al., 2020), this implies a density deficit far in excess of that observed in Earth's core (Birch, 1964). Taken at face value, it requires the incorporation of substantial amounts of light elements (LEs) into the martian core during the early stages of planetary formation (e.g., Khan et al., 2022; Steenstra & van Westrenen, 2018). Previous work that relied mostly on analyses of martian meteorites and cosmochemical arguments (e.g., Lodders & Fegley, 1997; Sanloup et al., 1999; Taylor, 2013; Wänke et al., 1994; Yoshizaki & McDonough, 2020), including geophysical data (Khan et al., 2022), and metal-silicate partitioning results (e.g., Brennan et al., 2020; Gendre et al., 2022; Rubie et al., 2004; Steenstra & van Westrenen, 2018; Wang & Becker, 2017), have suggested that Mars' core is rich in S, along with C, O and/or H. Silicon is considered negligible in the martian core, because of the relatively oxidized nature of the martian mantle (~ΔIW − 1) as inferred from the compositions of SNC meteorites (Shergottites, Nahklites, and Chassignites) and the correspondingly high mantle FeO content (Wadhwa, 2008; Yoshizaki & McDonough, 2020).

On the other hand, how the individual LE influences the seismic properties, such as density (ρ) and P-wave velocity (Vp) under relevant P-T conditions, is poorly explored. Relative to studies on Earth's liquid outer core (~100s GPa) (e.g., H. Huang et al., 2013; Morard et al., 2017) and small planetary cores (typically less than 10 GPa, see (Pommier et al., 2022) for a recent review), density or compressional sound velocity measurements on liquid

Fe-X mixtures, where X is either of the cosmochemically-relevant elements S, C, O, or H, are scarce and poorly agreed upon in the pressure range of Mars' core (~20–40 GPa). For example, there are five experimental studies to date on the liquid Fe(Ni)-S system that reported either ρ or Vp data in the aforementioned pressure range without extrapolation (Balog et al., 2003; Kawaguchi et al., 2017, 2022; Morard et al., 2013; Nishida et al., 2020). However, these studies report that S has opposing effects on Vp (Kawaguchi et al., 2017; Nishida et al., 2020), in which adding S to the Fe(Ni)-S binary causes both an increase and a decrease in Vp. In the liquid Fe-C system, only one study reports measurements of Vp in the pressure region of Mars' core (Nakajima et al., 2015). On the other hand, experiments at martian core pressures are presently unavailable in the liquid Fe-O and Fe-H systems. Despite the limited availability of experimental data, thermodynamic models that synthesize this information for the prediction of elastic properties (Rivoldini et al., 2011) have been widely used to infer the physical states and compositions of planetary cores (Khan et al., 2022; Terasaki et al., 2019). Inherent to these models, however, is the necessity to combine experimental measurements from a range of methodologies and approaches, each with their own uncertainty on the desired property (temperature, density, Vp) (e.g., Morard et al., 2007; Nishida et al., 2020; Stewart et al., 2007). It is therefore challenging to evaluate the random errors introduced by constructing such models from disparate measurements.

Ab initio calculations provide an alternative and complementary approach to obtaining the elastic properties of liquid Fe or Fe-X mixtures. They have the advantage of being performed within a single computational framework that thereby eliminates random errors associated with combining distinct experimental determinations of individual binary- or ternary systems. Yet, most ab initio calculations have focused on higher pressures than those relevant for the Martian core, with studies focusing on applying their results to the cores of the Earth (Badro et al., 2014; D. Huang et al., 2019; Ichikawa & Tsuchiya, 2020; Umemoto & Hirose, 2020) and super-Earths (Li et al., 2022; Wagle & Steinle-Neumann, 2019). Relatively few ab initio studies have focused on smaller planetary cores, partly because of the complex spin transitions that occur in *d*-orbital electrons in liquid Fe at lower pressures (Edgington et al., 2019; Morard et al., 2022).

In order to aid in resolving uncertainties among experimental datasets (Kawaguchi et al., 2017; Nishida et al., 2020; Poirier, 1994), as well as to provide a reference mineral physics database for studying the elastic properties of liquid metal cores of Mars- and Mercury-sized planets (~20–40 GPa), here we perform both non-spin- and spin-polarised ab initio calculations on liquid Fe-X mixtures, where X comprises Ni and the cosmochemically-favoured LEs S, C, O and H (Khan et al., 2022; Yoshizaki & McDonough, 2020).

2. Methods

2.1. Ab Initio Molecular Dynamics (AIMD) Simulations

AIMD simulations based on density functional theory (DFT) were performed using the Vienna Ab initio Simulation Package (Kresse & Hafner, 1993). A Perdew–Burke–Ernzerhof-type (Perdew et al., 1996) generalized gradient approximation (GGA) was used to treat the exchange-correlation functionals. Core radii and valence electronic configurations of candidate elements in the martian core (Fe, Ni, S, C, O and H) are reported in Table S1 in Supporting Information S1. The Brillouin zone was sampled with the Γ point, with a cutoff energy of 500 eV (or 600 eV for H-bearing supercells) for the plane-wave basis set. Pulay stress was evaluated to be less than 1 GPa with a higher cutoff energy of 700 eV and a $2 \times 2 \times 2$ k-point grid. A Nosé-Poincaré thermostat was used to control the temperature in the canonical ensemble (NVT).

A cubic box containing 108 atoms was first heated to 6000 K to obtain a liquid structure, then cooled down to two P-T conditions relevant to the martian core (19 GPa/2100 K and 35 GPa/2400 K), which correspond to the martian core-mantle-boundary (CMB) and ~1,200 km below it (~2,800 km depth from the surface), respectively (Khan et al., 2022). A number of different volumes, that is, densities, were carefully selected to encompass each of the above two anchored P-T conditions in a small range of ~5 GPa, to better resolve the influence of LEs at a given P and T. Simulations were run for 18–27 ps with a time step of 1 ps (0.5 ps for Fe-H binaries). A liquid structure was confirmed by the partial radial distribution function (RDF) and mean square displacement (MSD) (D. Huang et al., 2019). P and T were calculated from the time average discarding the first 1 ps. Using the blocking method (Flyvbjerg & Petersen, 1989), statistical uncertainties in pressure were evaluated to be between 0.1 and 0.2 GPa (Figure S1 in Supporting Information S1). Small statistical errors in pressure (<0.5 GPa) are achievable by increasing the precision of the ab initio calculations, as commonly seen in recent DFT work (Bajgain

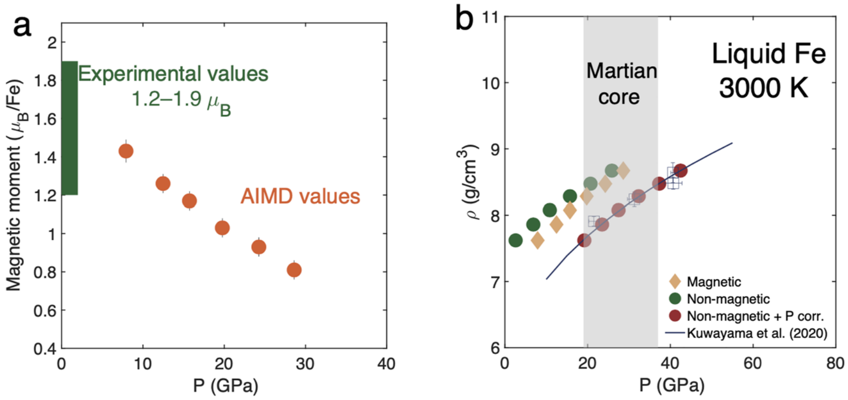

Figure 1. Benchmark calculations of liquid Fe at 3000 K. (a) Local magnetic moments calculated from unconstrained spin-polarised ab initio molecular dynamics simulations are shown using the Bohr magneton (μ_B) per Fe atom, along with experimental data at 1 bar and ~1900 K (Waseda & Suzuki, 1970; Weber et al., 1978). (b) Isothermal P-ρ equations of state (EoS) of liquid Fe at 3000 K. At similar densities, both magnetic (yellow diamonds) and non-magnetic (green dots) calculations underestimate pressure, relative to the EoS (blue line) based on recent density measurements (blue squares) (Kuwayama et al., 2020). After applying a constant pressure correction of 16.6 GPa to the non-magnetic calculations (green dots), the corrected EoS (red dots) agrees well with the diamond anvil cell experiments by Kuwayama et al. (2020). See main text for details.

et al., 2021; D. Huang et al., 2019). In order to investigate the influence of the size of the supercell on the results, we ran separate simulations in a larger supercell containing 216 Fe atoms for 8 ps using identical settings. As shown in Figure S2 and Table S2 in Supporting Information S1, the structure and elasticity of liquid Fe obtained with different supercell sizes are indistinguishable from each other.

2.2. Benchmark Calculations of Liquid Iron and Reproducibility of Experimental Data

It is known that AIMD simulations of the properties of Fe tend to underestimate pressure (i.e., overestimate density) (e.g., Alfè et al., 2002). The mismatch in pressure is due to the intrinsic assumptions of Perdew-Burke-Ernzerhof functionals and the common practice of non-spin-polarised treatment, whereas liquid Fe is in fact paramagnetic at low pressure (Waseda & Suzuki, 1970). To characterize the effect of the latter on the AIMD-derived equation of state (equations of state (EoS)) of pure Fe, we ran parallel simulations on both non-spin-polarised (non-magnetic) and unconstrained collinear spin-polarised (magnetic) Fe over a range of pressures, and compare the resulting densities with experimental data in Figure 1. We find (a) that the local magnetic moment in spin-polarised liquid Fe decreases with pressure, but persists in the pressure range of Mars's core (Figure 1a), and (b) negative correlation between the local magnetic moment and pressure underestimation (Figure 1b). Although more detailed treatment of the magnetic properties of iron does improve the agreement with experimentally determined densities, a considerable gulf remains between them. For instance, at 20 GPa and 3000 K, the inclusion of a magnetic entropy term in energy predicts a liquid Fe density of ~8.1 g/cm^3 (Edgington et al., 2019), which is 2% lower than our value of ~8.3 g/cm^3, yet higher by 5% than the experimental value of 7.7 g/cm^3 (Figure 1b); meanwhile, incorporating the magnetic entropy consistently overestimates the magnetic moment of pure Fe at 1 bar (Edgington et al., 2019). It is the unbalanced approximation of the exchange-correlation functional that accounts for such a mismatch.

In comparison with experiments, our simulations with both magnetic and non-magnetic configurations are seen to underestimate pressure, according to varying degrees of magnetic moment underestimation (Figure 1b). As a result, the magnetic calculations with higher magnetic moments provide an EoS closer to experimental data, consistent with the results of Edgington et al. (2019) and Morard et al. (2022). However, insofar as compressibility (in other words the curvature of the ρ-P curve, Figure 1b) is concerned, the magnetic EoS fails to reproduce the experimental data, necessitating a ρ-dependent correction to pressure to achieve agreement. The compressibility of Fe in non-magnetic simulations, in contrast, is seen to provide a good match to the experimentally-determined EoS of liquid iron (Kuwayama et al., 2020), indicating that the underestimated pressure is independent of ρ, allowing for the application of a constant pressure correction. We estimate the pressure correction to be 16.6 GPa over the pressure regime of Mars' core (19–37 GPa, Figure 1b). This is in line with (a) the observation that the difference between simulated and observed pressure becomes larger at lower pressures, for example, 8 GPa at Earth's inner-outer core boundary (330 GPa) and 10 GPa at its CMB (136 GPa) (Badro et al., 2014; Bajgain et al., 2021), and (b) a recent evaluation of a ρ-dependent pressure shift determined by comparing calculations to the density of *hcp* Fe and by benchmarking against that of liquid Fe at ambient pressure (Li et al., 2022), in the form of a sigmoid function $\Delta P = 17.38/(1 + \exp((\rho - 11.395) \cdot 1.341))$, which corresponds to a pressure correction of 17 ± 0.4 GPa in the density range of 6–9 g/cm^3.

The same pressure correction is applied to all the Fe-X systems studied here, because (a) LEs are generally thought to be present in Mars' core in low concentrations (except for S) and hence only marginally affect the bulk properties of Fe, and (b) direct comparison with experiments on liquid Fe-X alloys is rendered difficult by the lack of density data for a wide range of mixtures (see discussions in Section 1).

The robustness of our pressure-corrected non-spin-polarised calculations are supported by the fact that (a) the calculated densities of liquid Fe-S, and (b) the calculated sound velocities of liquid Fe and Fe-C reproduce available experimental data within uncertainties (Balog et al., 2003; Kawaguchi et al., 2017, 2022; Kuwayama et al., 2020; Morard et al., 2013; Nakajima et al., 2015; Nishida et al., 2020) as summarized in Figure 2. However, as regards Vp of liquid Fe-S binaries (Figure 2b), our results do not fully agree with experiments, where the effect of S on Vp of liquid Fe is either negligible or slightly negative at 19 GPa (Kawaguchi et al., 2017; Nishida et al., 2020). The mismatch may be due to the applied pressure correction (∼17 GPa), which is the same as the value used for liquid Fe. Meanwhile, in the case of Fe-C binaries, our Vp agrees well with experiments (Nakajima et al., 2015) as discussed above. This necessitates a species-dependent pressure correction, which is however currently unavailable because of the scarcity of experimental data (see Introduction for details).

The potential influence of element-dependent magnetism on liquid properties is obtained by comparing magnetic and non-magnetic simulations. The radial distribution functions for the spin- and non-spin-polarised simulations are shown in Figure 3 and illustrate structural similarities across all of the binary systems studied here. In general, at the same density, the spin-polarised treatment increases bond length, that is, the position of the first peak for each species in the partial radial distribution functions, and therefore yields higher pressures relative to the non-spin-polarised simulations. Bond length changes between non-magnetic to magnetic systems are summarized in Table S3 in Supporting Information S1. The biggest difference is seen to occur in the case of Fe-O system, where bond length change in the Fe-Fe bond between the two simulations is most noticeable. This generally agrees with the simulations of the Fe-O system conducted by Morard et al. (2022), with the exception that the larger absolute differences between their spin- and non-spin-polarised bond lengths relative to ours potentially relate to Morard et al. (2022) considering an Fe-O system with 50 mol% O. The shortest bond length among all bond pairs (Fe-Fe, Fe-X, X-X) is that of Fe-X, which barely changes for Fe-C and Fe-H, but increases by 0.05 Å for both Fe-O and Fe-S from non-spin-polarised to spin-polarised systems (Figure 3 and Table S3 in Supporting Information S1). Furthermore, except for slight decreases in peak intensity (and peak-shape-sharpening of the O-O pair), the S-S, C-C and H-H bonds (Table S3 in Supporting Information S1) are barely affected in going from non-spin- to spin-polarised simulations and amount to density differences (Table S4 in Supporting Information S1) that are consistently small for all considered systems (within 2%).

3. Results

3.1. Elastic Properties of Liquid Fe-X Under Mars' Core Conditions

3.1.1. Density and Incompressibility

The results from our AIMD simulations in the form of density and bulk sound velocity are shown in Figure 2, while volume and isothermal bulk modulus are shown in Figure S3 in Supporting Information S1. At the conditions of Mars' core, the addition of LEs invariably decreases the density of liquid Fe (Figures 2a and 2c), with S and O affecting density more than C and H on a molar basis; whereas the influence of Ni is negligible. This is consistent with previous simulations at the conditions of Earth's core in which the magnitude of the density reduction of iron diminishes following the sequence Si, S, O, C and H (Badro et al., 2014; D. Huang et al., 2019; Ichikawa & Tsuchiya, 2020; Umemoto & Hirose, 2020). This can be explained by the relative mass-to-volume (Δm/ΔV) change introduced by the incorporation of a LE. For example, interstitial H significantly reduces both volume (Figure S3a and S3c in Supporting Information S1) and mass, while C causes smaller Δm and ΔV than

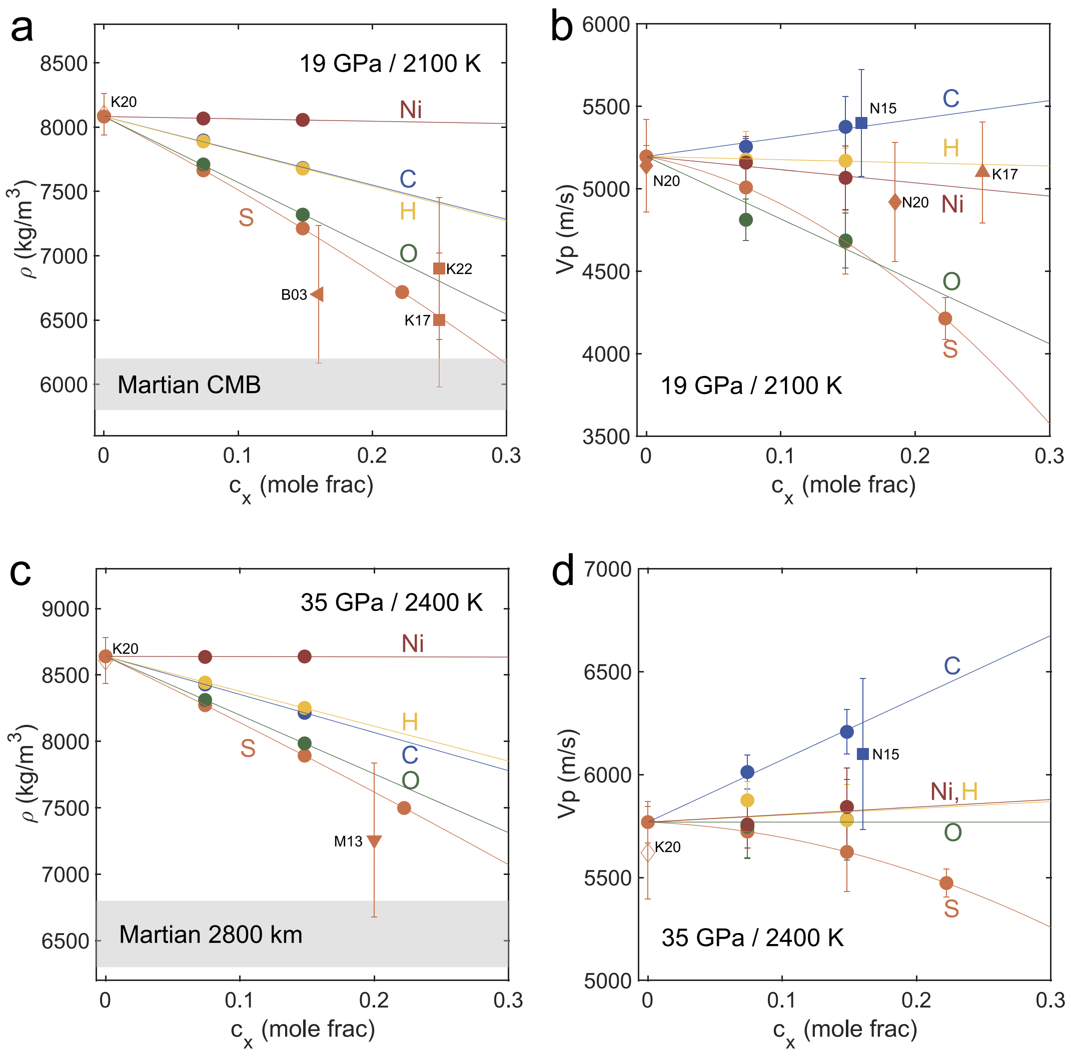

Figure 2. Density and bulk sound velocity of liquid Fe-X (X = Ni, S, O, C and H) as a function of X's concentration at conditions of the martian core-mantle-boundary (19 GPa / 2100 K) and within Mars' liquid core (35 GPa / 2400 K). Results from our ab initio molecular dynamics simulations are shown as solid circles. Experimental data for liquid Fe (K20 (Kuwayama et al., 2020) and N20 (Nishida et al., 2020)), Fe-S (B03 (Balog et al., 2003), M13 (Morard et al., 2013), K17 (Kawaguchi et al., 2017), N20 (Nishida et al., 2020) and K22 (Kawaguchi et al., 2022)) and Fe-C (N15 (Nakajima et al., 2015)) are shown as solid or open angular markers. Shaded gray areas are density values from literature (Khan et al., 2018; Rivoldini et al., 2011). Error bars are reported using 2σ for both calculations and experiments, and are visible when exceeding symbol size. Note that only experiments performed at high pressures encompassing Mars' core conditions (19–35 GPa) are compared here through interpolation; extrapolations from lower pressure are not considered due to the uncertainties associated with the extrapolation.

H, such that C and H have a near-identical effect (on a molar basis) on density reduction of liquid Fe (Figures 2a and 2c). Sulfur, on the other hand, expands the volume of liquid Fe, indicating substitutional occupancy with slightly larger atomic radius at these pressures (Ichikawa & Tsuchiya, 2020).

As indicated by the linear trends in Figure 2 and Figure S3 in Supporting Information S1, density and volume of the Fe-X binary system can be approximated from linear mixtures in the case of Ni, C, H and O, which agrees with results obtained at higher pressures (D. Huang et al., 2019). One of our Fe-O binaries, with 14.8 mol% O, is close to the immiscibility gap predicted in the liquid Fe-O system at 20 GPa and ~2,400 K (which closes at pressures higher than 25 GPa) (Frost et al., 2010), it is therefore expected to exhibit non-ideal mixing behavior in our simulations at 19 GPa, which apparently does not occur as discussed above. We conclude that in the investigated P-T-X range, that is, 19–35 GPa, 2100–2400 K with 0–14.8 mol% O, liquid Fe-O alloys mix ideally regarding volume and density. In agreement with observations at 1 bar (Komabayashi, 2021) and melting experiments at

10.1029/2022GL102271

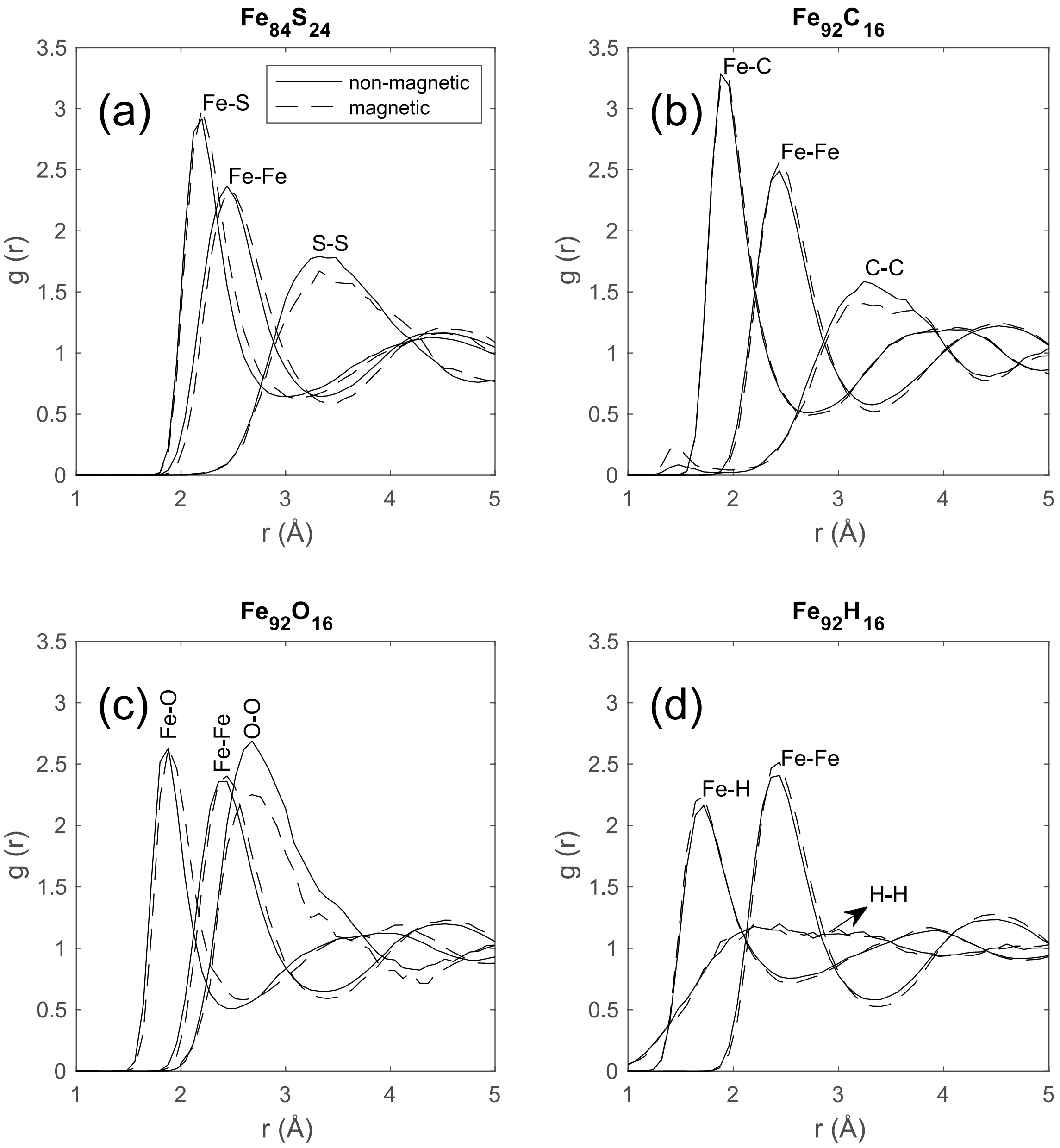

Figure 3. Partial radial distribution functions of Fe-S, Fe-C, Fe-O and Fe-H liquids based on spin- and non-spin-polarised ab initio molecular dynamics simulations at similar densities and a temperature of 2100 K. Densities are respectively 6.7, 7.7, 7.3 and 7.7 g/cm^3 for (a), (b), (c) and (d), which all correspond to 19 GPa after applying a pressure correction to the non-magnetic calculations (cf. Figure 2a). Bond length changes between non-magnetic and magnetic systems are summarized in Table S3 in Supporting Information S1.

higher pressures (Chen et al., 2008; Pease & Li, 2022; Pommier et al., 2018) that suggest non-ideality for the Fe-S system, we find that volume, density and compressibility cannot be accurately described by linear mixtures of liquid Fe and S (Figure 2 and Figure S3 in Supporting Information S1). The excess molar volume of mixing for Fe-S is taken into account in our mixing model and will be discussed below.

Based on the simulations performed around the two P-T conditions, we obtain the isothermal bulk modulus K_T by fitting the P-V data to a second-order Birch-Murnaghan (BM) EoS

$$P = \frac{3}{2}K_0\left[\left(\frac{V_0}{V}\right)^{\frac{7}{3}} - \left(\frac{V_0}{V}\right)^{\frac{5}{3}}\right]\left[1 + \frac{3}{4}\left(K_0' - 4\right)\left(\left(\frac{V_0}{V}\right)^{\frac{2}{3}} - 1\right)\right], \quad (1)$$

Table 1

Thermal Expansion Coefficient (α), Specific Heat Capacity (C_V), Grüneisen Parameter (γ), Isothermal Bulk Modulus (K_T), dK_T/dT, Isentropic Bulk Modulus (K_S), Density (ρ) and Bulk Sound Velocity (V_Φ) of Liquid Fe at the Two Locations in Mars' Core

Liquid Fe	CMB (19 GPa/2100 K)	1σ	2,789 km (35 GPa/2400 K)	1σ
α (K^{-1})	6.99E−05	2.9E−06	5.31E−05	3.3E−06
C_V (J/kg/K)	494	16	496	24
γ	2.74	0.14	2.66	0.20
K_T (GPa)	156	2	215	4
dK_T/dT (GPa/K)	−0.026	0.006	–	–
K_S (GPa)	218	3	288	5
ρ (kg/m^3)[a]	8,083	1	8,640	1
V_Φ (m/s)[a]	5,196	33	5,769	51

[a] Uncertainties in density and velocity are obtained by equation of state fitting (Equation 1) and subsequent error prorogation, which are smaller than their uncertainties in the mixing model (see below).

where K_0 is the isothermal bulk modulus, V_0 the reference volume at the pressures considered here (19 or 35 GPa), and K_0' is the derivative of the bulk modulus with respect to pressure, which, in the case of a second-order BM EoS, equals 4. Similar to density, S and O are seen in Figure S3 in Supporting Information S1 to have the strongest effect on decreasing the compressibility (K_T) of liquid Fe, whereas the effects of Ni and H are comparable, particularly at 19 GPa. Carbon is the only element that appears to make liquid Fe stiffer (higher K_T) at both pressures. Again, like density, the effect of X on K_T of Fe-X binaries is, within uncertainties, quasi-linear for Ni, C, H and O, but can be described more accurately by a polynomial fit for S (Figure S3 in Supporting Information S1).

3.1.2. Bulk Sound Velocity

In addition to the aforementioned simulations, we conducted calculations on liquid Fe at varying temperatures but constant volume at two reference conditions of Mars' core to obtain the thermal expansion coefficient (α), the specific heat capacity at constant volume (C_V) and the Grüneisen parameter (γ) through the relations

$$\alpha = \frac{1}{K_T}\left(\frac{\partial P}{\partial T}\right)_V, \tag{2}$$

$$C_V = \frac{1}{M}\left(\frac{\partial U}{\partial T}\right)_V, \tag{3}$$

$$\gamma = \frac{\alpha K_T}{C_V \rho}, \tag{4}$$

where M is the mass, U the internal energy of the system, and the subscript V denotes constant volume. The computed values for the thermodynamic parameters are listed in Table 1. From these, we can obtain the isentropic bulk modulus (K_S) and bulk sound velocity (V_Φ, which equals Vp in liquids) according to

$$K_S = (1 + \alpha\gamma T) \cdot K_T, \tag{5}$$

$$V_\Phi = \sqrt{\frac{K_S}{\rho}}. \tag{6}$$

The calculated velocities for the Fe-X mixtures considered here are shown and compared to available experiments in the 20–40 GPa pressure range for liquid Fe (Kuwayama et al., 2020; Nishida et al., 2020), Fe-C (Nakajima et al., 2015) and Fe-S (Kawaguchi et al., 2017; Nishida et al., 2020) in Figure 2b. By comparing with recent ab initio results obtained at conditions of Earth's outer core (Badro et al., 2014; D. Huang et al., 2019; Ichikawa & Tsuchiya, 2020; Umemoto & Hirose, 2020), we are able to identify a low-P versus high-P dichotomy in the elastic properties of liquid Fe-X alloys. The addition of LEs is in general expected to decrease the density more than it is the bulk modulus, and thus the liquid Fe-X mixtures should have higher velocities (Brodholt & Badro, 2017). This is the case at high pressures relevant to Earth's core (D. Huang et al., 2019; Bajgain et al., 2021); however at the pressure-temperature conditions in cores of Mars- and Mercury-sized planets, the negative effect of LEs in Fe-X alloys holds for density, but not for elastic properties (bulk modulus and velocity). The latter depend on composition and pressure: (a) at the martian CMB (19 GPa), the addition of S, O or H, decreases velocity, because it changes (decreases) K_T more than it does density, for example, the incorporation of 22 mol% S in liquid Fe decreases K_T by 50%, and density by only 20% (Figures 2a and 2b and Figure S3b in Supporting Information S1); and (b) at 19 GPa, O strongly reduces bulk sound velocity (Figure 2b), whereas at 35 GPa, its influence on density and K_T becomes comparable (Figure 2c and Figure S3d in Supporting Information S1), hence the velocity change induced by O is no longer as pronounced (Figure 2d). At the two P-T conditions, where our simulations are anchored, C remains the only LE that can raise bulk sound velocity above that of pure liquid Fe, because it simultaneously decreases the density and increases the bulk modulus of the binary mixture.

3.2. Non-Ideality of Liquid Fe-S Alloy and Validation of Mixing Model

Because of the challenging nature of high-pressure experiments, on the one hand, and the ensuing scarcity of available data under extreme P-T conditions relevant to the interior of Earth-sized planets, on the other, ideal mixing of binary liquid Fe-X alloys has been widely assumed (e.g., Badro et al., 2014; Komabayashi, 2021; Morard et al., 2018; Poirier, 1994) as a means of evaluating elastic properties of multi-component Fe-rich liquids. While ideal mixing has been confirmed at conditions of Earth's core (D. Huang et al., 2019; Umemoto & Hirose, 2020), our low-pressure simulations show non-ideal (i.e., non-linear) behavior of density and compressibility upon the mixing of Fe and S (Figure 2 and Figure S3 in Supporting Information S1), which, when combined with the non-ideal liquidus curve found for the Fe-S system (Chen et al., 2008), clearly shows that the Fe-S non-ideality (in the Fe-rich portion of the Fe-S binary) persists across the pressure range covering Mars' core. Analogous to the Earth, Mars' liquid core is likely a mixture of Fe and multiple LEs (Khan et al., 2022) and we therefore design a mixing model to utilize our calculated binary properties as follows.

At a given depth, that is, fixed P and T, the seismic properties of an Fe-X mixture, determined solely by its composition, are calculated from

$$\rho_{mix}(x_i) = \rho_{Fe} + \sum_{i}^{n} \int_{0}^{x_i} \frac{\partial \rho}{\partial x_i} dx_i, \tag{7}$$

and

$$K_{T_{mix}}(x_i) = K_{T_{Fe}} + \sum_{i}^{n} \int_{0}^{x_i} \frac{\partial K_T}{\partial x_i} dx_i, \tag{8}$$

where x_i is the concentration (in molar fraction) of the impurity elements ($n = 5$, viz. Ni, S, O, C and H). Partial derivatives of ρ and K_T with respect to x_i ($\frac{\partial \rho}{\partial x_i}$ and $\frac{\partial K_T}{\partial x_i}$) are constants for Ni, O, C and H, except for S because of its non-linear behavior (Table S5 in Supporting Information S1). The P-wave velocity of the mixture is then calculated from Equations 5 and 6 using the parameter values reported in Table 1. Here, we assume that the thermal expansion coefficient (α) and the Grüneisen parameter (γ) are independent of x_i (species and concentration of the impurity element). This is supported by the negligible change (within uncertainties) of α and γ when LEs are added to liquid Fe (D. Huang, 2019).

To validate our mixing model that takes account of the non-ideality of the Fe-S binary, we ran additional calculations on two Fe-S-C ternaries ($Fe_{100}S_4C_4$ and $Fe_{92}S_8C_8$). The calculated ρ, K_T and V_Φ at martian CMB conditions (19 GPa and 2100 K) are identical to the values obtained from our non-ideal mixing model within 2σ (Figure 4). This confirms the effectiveness of the non-ideal mixing model for Mars' core properties within the non-magnetic framework of the ab-initio calculations.

3.3. Implications for the Light-Element Content of the Martian Core

For the purpose of illustration, we consider an end-member scenario, wherein Mars' core is comprised of a binary mixture, that is, iron and one of the four cosmochemically-favored light-element candidates (S, C, O and H). Note that because the Fe-Ni system remains ideal in the case of density over the investigated pressure range (Figures 2a and 2c), it is reasonable to discuss the density of an Fe-X binary core without incorporating Ni. From the relation

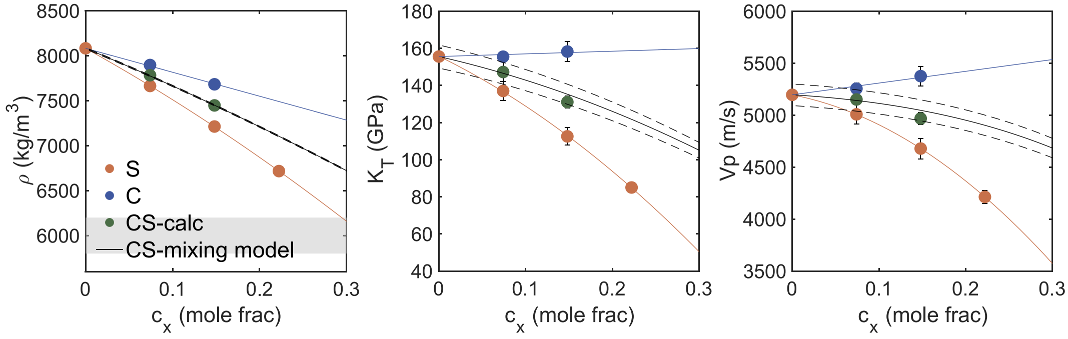

Figure 4. Comparison of calculated and mixed properties of liquid Fe-S-C alloys at martian core-mantle-boundary conditions (19 GPa and 2100 K). Shaded gray area is the target density range as in Figure 2. Ternary calculations for $Fe_{100}S_4C_4$ and $Fe_{92}S_8C_8$ are shown as solid green circles and are seen to be in agreement with our mixing model (solid lines, Equations 6–8) within 2σ (dashed lines).

$$X_i = \left[\frac{M_{Fe}}{M_i} \cdot \frac{1}{x_i} + 1\right]^{-1} \tag{9}$$

where M_i and M_{Fe} are molar masses of element i and Fe, respectively, and X_i and x_i are weight and mole fraction of element i, respectively, we are able to obtain a lower bound on the concentration of light components needed to match the seismically-inferred mean core density (Drilleau et al., 2022; Durán et al., 2022; Khan et al., 2022; Stähler et al., 2021). Depending on mantle temperature, the estimated densities at 19 GPa (core side of the martian CMB) and 35 GPa (~1,200 km below the CMB) are in the ranges 5.8–6.2 g/cm^3 and 6.3–6.8 g/cm^3, respectively (Bagheri et al., 2019; Khan et al., 2018). To reach the density deficit (~2 g/cm^3) needed to fit the observed mean core density, a binary core would require at least 30 mol% (~20 wt%) S estimated from the data at 19 GPa, or 40 mol% (~30 wt%) S estimated from those at 35 GPa (Figure 2).

If our simulated temperature (2,100 K) at 19 GPa overestimates core temperature, this would imply that an even larger amount of S is needed to match density since the deficit would increase. Given that S, among all considered elements most efficiently reduces density of liquid Fe, 40 mol% serves as the lower bound for the amount of any LE needed to match Mars' mean core density. This is in contrast to Earth's core, where a maximum of ~35 mol% LE (upper bound set by H (Umemoto & Hirose, 2020)) is required to match the preliminary reference Earth model density profile (Dziewonski & Anderson, 1981). Relative to the Earth, this points to a volatile-rich Mars, because S alone would make up 7.5 wt% of the whole planet (30 wt% S in a core which is 25% of Mars's total mass (Stähler et al., 2021)), assuming S to be the primary LE. However, such a high abundance of S alone in bulk Mars is forbidden by the volatile content inferred from moderately volatile lithophile elements (Khan et al., 2022). This indicates that Mars' core is enriched also in C, O or H, in addition to S.

4. Conclusions

We performed DFT-based molecular dynamics simulations on liquid Fe-X binaries, where X = Ni, S, C, O or H, to investigate how composition influences the thermoelastic properties of liquid iron under P-T conditions relevant to Mars' core. Relative to non-magnetic simulations, magnetic calculations bring the equation of state for liquid Fe slightly closer to the experiments, but predict a less accurate compressibility for liquid Fe. As concerns volume, density, and isothermal bulk modulus, Ni, C, O and H are found to mix ideally with liquid Fe, while the Fe-S binary system shows well-defined non-ideality. All the investigated LEs act to reduce the density of iron. Of these, S and O are most effective (on a molar basis) at reducing the density of pure liquid Fe. Unlike in the core of the Earth, the addition of LEs in small planetary cores (e.g., Mars or Mercury), does not necessarily result in a decrease of the bulk modulus of liquid Fe, but depends on the identity of the LE. We further validated a mixing model that incorporates the non-ideality of the Fe-S system, which may be used in the future to explore core compositions/properties containing multiple LEs. By comparing with the seismically-determined mean martian core density, we conclude that Mars' core is enriched in LEs, which readily makes the core a large reservoir for S, C, O or H.

Data Availability Statement

Ab initio molecular dynamics data are available in the repository Mendeley Data (https://data.mendeley.com/datasets/z68hmwvs8z) with https://doi.org/10.17632/z68hmwvs8z.1.

Acknowledgments

The AIMD simulations were supported by grants from the Swiss National Supercomputing Centre (CSCS) under project ID sm65. We thank two anonymous reviewers for their constructive and impartial comments. We appreciate the efficient editorial handling of Quentin Williams. M.M. acknowledges support from the ETH startup fund (PSP1-001828-000). A.K., D.G., and M.M. acknowledge support from the ETH+ funding scheme (ETH+02 19-1: "Planet Mars"). P.A.S. was supported by a Swiss National Science Foundation (SNSF) Ambizione Fellowship #180025 and the Swiss State Secretariat for Education, Research and Innovation (SERI) under contract number MB22.00033, a SERI-funded ERC Starting Grant "2ATMO."

References

Alfè, D., Price, G. D., & Gillan, M. J. (2002). Iron under Earth's core conditions: Liquid-state thermodynamics and high-pressure melting curve from ab initio calculations. *Physical Review B*, *65*(16), 165118. https://doi.org/10.1103/PhysRevB.65.165118

Badro, J., Cote, A. S., & Brodholt, J. P. (2014). A seismologically consistent compositional model of Earth's core. *Proceedings of the National Academy of Sciences*, *111*(21), 7542–7545. https://doi.org/10.1073/pnas.1316708111

Bagheri, A., Khan, A., Al-Attar, D., Crawford, O., & Giardini, D. (2019). Tidal response of Mars constrained from laboratory-based viscoelastic dissipation models and geophysical data. *Journal of Geophysical Research: Planets*, *124*(11), 2703–2727. https://doi.org/10.1029/2019je006015

Bajgain, S. K., Mookherjee, M., & Dasgupta, R. (2021). Earth's core could be the largest terrestrial carbon reservoir. *Communications Earth & Environment*, *2*(1), 165. https://doi.org/10.1038/s43247-021-00222-7

Balog, P. S., Secco, R. A., Rubie, D. C., & Frost, D. J. (2003). Equation of state of liquid Fe-10 wt % s: Implications for the metallic cores of planetary bodies. *Journal of Geophysical Research: Solid Earth*, *108*(B2). https://doi.org/10.1029/2001JB001646

Banerdt, W. B., Smrekar, S. E., Banfield, D., Giardini, D., Golombek, M., Johnson, C. L., et al. (2020). Initial results from the InSight mission on Mars. *Nature Geoscience*, *13*(3), 183–189. https://doi.org/10.1038/s41561-020-0544-y

Birch, F. (1964). Density and composition of mantle and core. *Journal of Geophysical Research*, *69*(20), 4377–4388. https://doi.org/10.1029/JZ069i020p04377

Brennan, M. C., Fischer, R. A., & Irving, J. C. (2020). Core formation and geophysical properties of Mars. *Earth and Planetary Science Letters*, *530*, 115923. https://doi.org/10.1016/j.epsl.2019.115923

Brodholt, J., & Badro, J. (2017). Composition of the low seismic velocity E′ layer at the top of Earth's core. *Geophysical Research Letters*, *44*(16), 8303–8310. https://doi.org/10.1002/2017GL074261

Chen, B., Li, J., & Hauck, S. A., II. (2008). Non-ideal liquidus curve in the Fe-S system and Mercury's snowing core. *Geophysical Research Letters*, *35*(7). https://doi.org/10.1029/2008GL033311

Drilleau, M., Samuel, H., Garcia, R. F., Rivoldini, A., Perrin, C., Michaut, C., et al. (2022). Marsquake locations and 1-D seismic models for Mars from InSight data. *Journal of Geophysical Research: Planets*, *127*(9), e2021JE007067. https://doi.org/10.1029/2021JE007067

Durán, C., Khan, A., Ceylan, S., Zenhäusern, G., Stähler, S., Clinton, J., & Giardini, D. (2022). Seismology on Mars: An analysis of direct, reflected, and converted seismic body waves with implications for interior structure. *Physics of the Earth and Planetary Interiors*, *325*, 106851. https://doi.org/10.1016/j.pepi.2022.106851

Dziewonski, A. M., & Anderson, D. L. (1981). Preliminary reference Earth model. *Physics of the Earth and Planetary Interiors*, *25*(4), 297–356. https://doi.org/10.1016/0031-9201(81)90046-7

Edgington, A., Vočadlo, L., Stixrude, L., Wood, I., Dobson, D., & Holmström, E. (2019). The top-down crystallisation of Mercury's core. *Earth and Planetary Science Letters*, *528*, 115838. https://doi.org/10.1016/j.epsl.2019.115838

Flyvbjerg, H., & Petersen, H. G. (1989). Error estimates on averages of correlated data. *The Journal of Chemical Physics*, *91*(1), 461–466. https://doi.org/10.1063/1.457480

Frost, D. J., Asahara, Y., Rubie, D. C., Miyajima, N., Dubrovinsky, L. S., Holzapfel, C., et al. (2010). Partitioning of oxygen between the Earth's mantle and core. *Journal of Geophysical Research: Solid Earth*, *115*(2), 1–14. https://doi.org/10.1029/2009JB006302

Gendre, H., Badro, J., Wehr, N., & Borensztajn, S. (2022). Martian core composition from experimental high-pressure metal-silicate phase equilibria. *Geochemical Perspectives Letters*, *21*, 42–46. https://doi.org/10.7185/geochemlet.2216

Huang, D. (2019). Experimental and theoretical investigation of core-mantle interations. (Doctoral dissertation). Sciences de la terre et de l'environnement Université Paris Cité 2019. Retrieved from http://www.theses.fr/2019UNIP7072

Huang, D., Badro, J., Brodholt, J., & Li, Y. (2019). Ab initio molecular dynamics investigation of molten Fe–Si–O in Earth's core. *Geophysical Research Letters*, *46*(12), 6397–6405. https://doi.org/10.1029/2019GL082722

Huang, H., Wu, S., Hu, X., Wang, Q., Wang, X., & Fei, Y. (2013). Shock compression of Fe-FeS mixture up to 204 GPa. *Geophysical Research Letters*, *40*(4), 687–691. https://doi.org/10.1002/grl.50180

Ichikawa, H., & Tsuchiya, T. (2020). Ab initio thermoelasticity of liquid iron-nickel-light element alloys. *Minerals*, *10*(1), 59. https://doi.org/10.3390/min10010059

Kawaguchi, S. I., Morard, G., Kuwayama, Y., Hirose, K., Hirao, N., & Ohishi, Y. (2022). Density determination of liquid iron-nickel-sulfur at high pressure. *American Mineralogist*, *107*(7), 1254–1261. https://doi.org/10.2138/am-2021-7924

Kawaguchi, S. I., Nakajima, Y., Hirose, K., Komabayashi, T., Ozawa, H., Tateno, S., et al. (2017). Sound velocity of liquid fe-ni-s at high pressure. *Journal of Geophysical Research: Solid Earth*, *122*(5), 3624–3634. https://doi.org/10.1002/2016JB013609

Khan, A., Liebske, C., Rozel, A., Rivoldini, A., Nimmo, F., Connolly, J. A. D., et al. (2018). A geophysical perspective on the bulk composition of Mars. *Journal of Geophysical Research: Planets*, *123*(2), 575–611. https://doi.org/10.1002/2017JE005371

Khan, A., Sossi, P., Liebske, C., Rivoldini, A., & Giardini, D. (2022). Geophysical and cosmochemical evidence for a volatile-rich Mars. *Earth and Planetary Science Letters*, *578*, 117330. https://doi.org/10.1016/j.epsl.2021.117330

Komabayashi, T. (2021). Phase relations of Earth's core-forming materials. *Crystals*, *11*(6), 581. https://doi.org/10.3390/cryst11060581

Kresse, G., & Hafner, J. (1993). Ab initio molecular dynamics for liquid metals. *Physical Review B*, *47*(1), 558–561. https://doi.org/10.1103/PhysRevB.47.558

Kuwayama, Y., Morard, G., Nakajima, Y., Hirose, K., Baron, A. Q. R., Kawaguchi, S. I., et al. (2020). Equation of state of liquid iron under extreme conditions. *Physical Review Letters*, *124*(16), 165701. https://doi.org/10.1103/PhysRevLett.124.165701

Li, Q., Xian, J.-W., Zhang, Y., Sun, T., & Vočadlo, L. (2022). Thermal properties of liquid iron at conditions of planetary cores. *Journal of Geophysical Research: Planets*, *127*(4), e2021JE007015. https://doi.org/10.1029/2021JE007015

Lodders, K., & Fegley, B. (1997). An oxygen isotope model for the composition of Mars. *Icarus*, *126*(2), 373–394. https://doi.org/10.1006/icar.1996.5653

Morard, G., Antonangeli, D., Bouchet, J., Rivoldini, A., Boccato, S., Miozzi, F., et al. (2022). Structural and electronic transitions in liquid FeO under high pressure. *Journal of Geophysical Research: Solid Earth*, *127*(11), e2022JB025117. https://doi.org/10.1029/2022JB025117

Morard, G., Bouchet, J., Rivoldini, A., Antonangeli, D., Roberge, M., Boulard, E., et al. (2018). Liquid properties in the Fe-FeS system under moderate pressure: Tool box to model small planetary cores. *American Mineralogist*, *103*(11), 1770–1779. https://doi.org/10.2138/am-2018-6405

Morard, G., Nakajima, Y., Andrault, D., Antonangeli, D., Auzende, A. L., Boulard, E., et al. (2017). Structure and density of Fe-C liquid alloys under high pressure. *Journal of Geophysical Research: Solid Earth*, *122*(10), 7813–7823. https://doi.org/10.1002/2017JB014779

Morard, G., Sanloup, C., Fiquet, G., Mezouar, M., Rey, N., Poloni, R., & Beck, P. (2007). Structure of eutectic Fe–FeS melts to pressures up to 17 GPa: Implications for planetary cores. *Earth and Planetary Science Letters*, *263*(1), 128–139. https://doi.org/10.1016/j.epsl.2007.09.009

Morard, G., Siebert, J., Andrault, D., Guignot, N., Garbarino, G., Guyot, F., & Antonangeli, D. (2013). The Earth's core composition from high pressure density measurements of liquid iron alloys. *Earth and Planetary Science Letters*, *373*, 169–178. https://doi.org/10.1016/j.epsl.2013.04.040

Nakajima, Y., Imada, S., Hirose, K., Komabayashi, T., Ozawa, H., Tateno, S., et al. (2015). Carbon-depleted outer core revealed by sound velocity measurements of liquid iron–carbon alloy. *Nature Communications*, *6*(1), 8942. https://doi.org/10.1038/ncomms9942

Nishida, K., Shibazaki, Y., Terasaki, H., Higo, Y., Suzuki, A., Funamori, N., & Hirose, K. (2020). Effect of sulfur on sound velocity of liquid iron under Martian core conditions. *Nature Communications*, *11*(1), 1954. https://doi.org/10.1038/s41467-020-15755-2

Pease, A., & Li, J. (2022). Liquidus determination of the Fe-S and (Fe, Ni)-S systems at 14 and 24 GPa: Implications for the Mercurian core. *Earth and Planetary Science Letters*, *599*, 117865. https://doi.org/10.1016/j.epsl.2022.117865

Perdew, J. P., Burke, K., & Ernzerhof, M. (1996). Generalized gradient approximation made simple. *Physical Review Letters*, *77*(18), 3865–3868. https://doi.org/10.1103/PhysRevLett.77.3865

Poirier, J.-p. (1994). Light elements in the Earth's outer core: A critical review. *Physics of the Earth and Planetary Interiors*, *85*(94), 9201–337. https://doi.org/10.1016/0031-9201(94)90120-1

Pommier, A., Driscoll, P. E., Fei, Y., & Walter, M. J. (2022). Investigating metallic cores using experiments on the physical properties of liquid iron alloys. *Frontiers in Earth Science*, *10*. https://doi.org/10.3389/feart.2022.956971

Pommier, A., Laurenz, V., Davies, C. J., & Frost, D. J. (2018). Melting phase relations in the Fe-S and Fe-S-O systems at core conditions in small terrestrial bodies. *Icarus*, *306*, 150–162. https://doi.org/10.1016/j.icarus.2018.01.021

Rivoldini, A., Van Hoolst, T., Verhoeven, O., Mocquet, A., & Dehant, V. (2011). Geodesy constraints on the interior structure and composition of Mars. *Icarus*, *213*(2), 451–472. https://doi.org/10.1016/j.icarus.2011.03.024

Rubie, D. C., Gessmann, C. K., & Frost, D. J. (2004). Partitioning of oxygen during core formation on the Earth and Mars. *Nature*, *429*(6987), 58–61. https://doi.org/10.1038/nature02473

Sanloup, C., Jambon, A., & Gillet, P. (1999). A simple chondritic model of Mars. *Physics of the Earth and Planetary Interiors*, *112*(1), 43–54. https://doi.org/10.1016/S0031-9201(98)00175-7

Stähler, S. C., Khan, A., Banerdt, W. B., Lognonné, P., Giardini, D., Ceylan, S., et al. (2021). Seismic detection of the martian core. *Science*, *373*(6553), 443–448. https://doi.org/10.1126/science.abi7730

Steenstra, E. S., & van Westrenen, W. (2018). A synthesis of geochemical constraints on the inventory of light elements in the core of Mars. *Icarus*, *315*, 69–78. https://doi.org/10.1016/j.icarus.2018.06.023

Stewart, A. J., Schmidt, M. W., van Westrenen, W., & Liebske, C. (2007). Mars: A new core-crystallization regime. *Science*, *316*(5829), 1323–1325. https://doi.org/10.1126/science.1140549

Taylor, G. J. (2013). The bulk composition of Mars. *Geochemistry*, *73*(4), 401–420. https://doi.org/10.1016/j.chemer.2013.09.006

Terasaki, H., Rivoldini, A., Shimoyama, Y., Nishida, K., Urakawa, S., Maki, M., et al. (2019). Pressure and composition effects on sound velocity and density of core-forming liquids: Implication to core compositions of terrestrial planets. *Journal of Geophysical Research: Planets*, *124*(8), 2272–2293. https://doi.org/10.1029/2019JE005936

Umemoto, K., & Hirose, K. (2020). Chemical compositions of the outer core examined by first principles calculations. *Earth and Planetary Science Letters*, *531*, 116009. https://doi.org/10.1016/j.epsl.2019.116009

Wadhwa, M. (2008). Redox conditions on small bodies, the Moon and Mars. *Reviews in Mineralogy and Geochemistry*, *68*(1), 493–510. https://doi.org/10.2138/rmg.2008.68.17

Wagle, F., & Steinle-Neumann, G. (2019). Liquid iron equation of state to the terapascal regime from ab initio simulations. *Journal of Geophysical Research: Solid Earth*, *124*(4), 3350–3364. https://doi.org/10.1029/2018JB016994

Wang, Z., & Becker, H. (2017). Chalcophile elements in martian meteorites indicate low sulfur content in the martian interior and a volatile element-depleted late veneer. *Earth and Planetary Science Letters*, *463*, 56–68. https://doi.org/10.1016/j.epsl.2017.01.023

Wänke, H., Dreibus, G., Wright, I. P., Cowley, S. W. H., Runcorn, S. K., & Southwood, D. J. (1994). Chemistry and accretion history of Mars. *Philosophical Transactions of the Royal Society of London. Series A: Physical and Engineering Sciences*, *349*(1690), 285–293. https://doi.org/10.1098/rsta.1994.0132

Waseda, Y., & Suzuki, K. (1970). Atomic distribution and magnetic moment in liquid iron by neutron diffraction. *physica status solidi (b)*, *39*(2), 669–678. https://doi.org/10.1002/pssb.19700390235

Weber, M., Knoll, W., & Steeb, S. (1978). Magnetic small-angle scattering from molten elements iron, cobalt, and nickel. *Journal of Applied Crystallography*, *11*(5), 638–641. https://doi.org/10.1107/S0021889878014107

Yoshizaki, T., & McDonough, W. F. (2020). The composition of Mars. *Geochimica et Cosmochimica Acta*, *273*, 137–162. https://doi.org/10.1016/j.gca.2020.01.011